PAPER

Check for updates

Detection of nitrophenols with a fluorescent Zr(IV) metal–organic framework functionalized with benzylamino groups†

Amina Chatz-Giachia, [ID] [a] Athanasia E. Psalti, [ID] [a] Anastasia D. Pournara,[b] Manolis J. Manos, [ID] [bc] Christina Pappa, [ID] [a] Konstantinos Triantafyllidis [ID] [a] and Theodore Lazarides [ID] *[a]

Nitroaromatic compounds (NACs) are known explosives and environmental pollutants posing a risk for public health and national security. Thus, the development of efficient sensors for their rapid and efficient in-field detection is of high importance. Analytical methods based on fluorescence are gaining interest as current light detection technology allows the fabrication of miniaturized portable devices suitable for in-field use. Herein, we report the rational design and synthesis of **Zr-1**, a Zr(IV) based metal–organic framework (MOF) which is structurally analogous to UiO-66 with the assigned formula $\{Zr_6O_4(OH)_8(H_2O)_4(\textbf{L-1})_{4-x}(NH_2bdc)_x\}$, (**L-1** = 2-((benzyl)amino)-terephthalate; NH_2bdc^{2-} = 2-aminoterephthalate). **Zr-1** incorporates a fluorescent ligand (**L-1**) with a pendant π-electron rich aromatic group and a basic secondary amine functionality, thereby targeting the selective detection of electron deficient and acidic NACs, 2,4,6-trinitrophenol (TNP) and 2,4-dinitrophenol (DNP). The stability of **Zr-1** in an aqueous environment was confirmed by powder X-ray diffraction analysis on water treated samples. Fluorescence titration experiments on aqueous suspensions of acid activated **Zr-1** (**pZr-1**) demonstrate that the material responds to small concentrations of TNP and DNP by displaying strong emission quenching, even in the presence of potentially competing compounds. The estimated limits of detection were found to be as low as 0.011 μM (2.5 ppb) for TNP and 0.026 μM (4.8 ppb) for DNP.

Introduction

Nitroaromatic compounds (NACs) are among the most important groups of industrial chemicals as they are widely used precursors and/or intermediates in the preparation of a variety of chemical products including pesticides, explosives, and pharmaceuticals. They are potently toxic and/or carcinogenic compounds with a highly explosive nature and their extensive industrial use renders them widely distributed environmental pollutants presenting a considerable danger to human population. Furthermore, NACs constitute one of the main ingredients for the preparation of explosive devices, thereby posing a major human safety and national security risk. NACs are xenobiotics resistant to chemical and biological oxidation and hydrolysis due to the electron-withdrawing character of nitro groups. Consequently, they

are persistent contaminants of soil, groundwater and wastewater, and their constant monitoring is indispensable for the protection and safeguarding of the environment.[1] Presently, determination of NACs is based mainly on traditional separation (*i.e.* GC, HPLC) and spectrometric (*i.e.* MS, IMS, IR) techniques, while their in-field detection is dominated by the use of trained canines. Despite their effectiveness, traditional analytical methods suffer from high cost, the requirement for highly trained personnel and lack of portability.[2]

In search of more convenient and cost-effective alternatives, great attention is directed to luminescence-based techniques that employ fluorescent materials as sensing elements. These sensors respond to their interaction with targeted analytes by producing detectable changes in their emission characteristics (*i.e.* emission intensity, wavelength of emission maxima, quantum yield). The advances in light generation and detection technologies allow detection limits at the single-molecule level to be easily attainable. Furthermore, device miniaturization is feasible, thereby allowing the potential development of small, portable, and user-friendly systems suitable for in-field use.[3]

Organic Conjugated Polymers (CPs) have been successfully employed in building optical sensors for nitro-explosives.

[a] *Department of Chemistry, Aristotle University of Thessaloniki, 54124 Thessaloniki, Greece. E-mail: tlazarides@chem.auth.gr*

[b] *Department of Chemistry, University of Ioannina, 45110 Ioannina, Greece*

[c] *Institute of Materials Science and Computing, University Research Center of Ioannina, 45110 Ioannina, Greece*

† Electronic supplementary information (ESI) available. See DOI: https://doi.org/10.1039/d2tc02494b

This journal is © The Royal Society of Chemistry 2022

J. Mater. Chem. C, 2022, **10**, 12307–12315 | **12307**

Swager and Yang first reported the synthesis of luminescent polymeric films displaying high sensitivity towards TNT and DNT.[4] Conjugated polymers provide a key advantage for optical sensing applications: the polymer chain, featuring multiple interconnected chromophores, provides a platform with high exciton mobility. The energy migration processes that occur in such systems amplify the material's response, as a single analyte binding event may affect a large number of chromophores thereby resulting in greatly enhanced detection signals.[5] This is in contrast to sensors which are based on small molecules, where each analyte binding event essentially only affects one chromophore.[6]

Luminescent Metal Organic Frameworks (LMOFs) is another promising class of luminescent materials that produce signal gain upon interaction with analytes.[7] MOFs are crystalline porous organic/inorganic hybrid materials that can be self-assembled from their corresponding metal ions/clusters and organic bridging ligands.[8] The introduction of luminescent properties in MOFs can be achieved by incorporation of fluorescent bridging ligands and/or photoactive metal anions in their framework, that leads to infinite arrays of chromophores, analogous to what is observed for CPs.[9] Moreover, MOFs exhibit well defined crystalline structures with permanent porosity, structural diversity and tunability, and surface functionality that distinguishes them from luminescent organic CP sensors. Luminescent MOFs can respond to the encapsulation of various guest species within their structure's pores and therefore, display great potential for use in next generation sensing devices for in-field detection.[10] In recent years, they have been extensively studied as optical sensors, however, relatively few research works focus on the rational design of MOF's pores structural design with the employment of tailored functional ligands.[11]

Herein, we study the rational design and synthesis of a hydrolytically stable Zr(IV) UiO-type[12] MOF with an average connectivity of 8 (**Zr-1**), based on a strongly fluorescent dicarboxylic ligand with a pendant π-electron rich benzylamino aromatic group (**L-1**). The incorporation of **L-1** into the MOF structure yields a material with pores lined with π-electron rich units, which, in combination with the basic amino groups, form a favourable environment for electron-deficient and acidic nitroaromatic guests. Fluorescence titrations with suspensions of protonated **Zr-1** (**pZr-1**) and 2,4-dinitrophenol (DNP) and 2,4,6-trinitrophenol (TNP),‡ have shown that our material can act as an efficient and selective optical sensor for the determination of these analytes in water displaying emission quenching with exceptionally low detection limits.
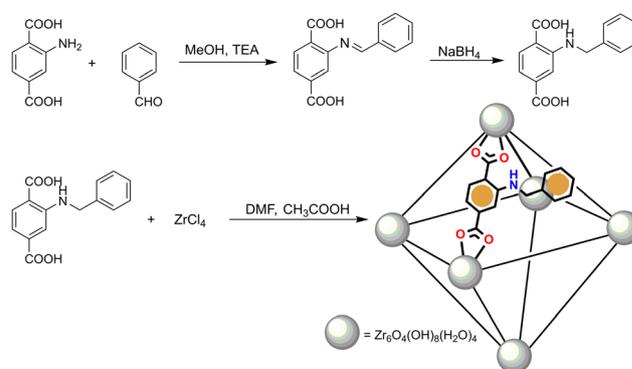
Results and discussion

Synthesis and characterization

We synthesized the porous Zr^{4+} MOF **Zr-1** using the functionalized dicarboxylic ligand 2-benzylaminoterephthalic acid, **L-1**. The syntheses of **L-1** and **Zr-1** are summarized in Scheme 1.

‡ Caution: This work involves the study of nitroaromatic compounds which are toxic and potentially explosive. To avoid the risk of explosion, nitroaromatics should only be handled in small quantities and in aqueous solution. Gloves and appropriate eyes and face protection should be worn at all times.

L-1 was prepared in a two-step process previously reported by our group[13] using the approach of reductive alkylation whereby the reaction of 2-aminorerephthalic acid with benzaldehyde affords an intermediate imine which is reduced in situ with sodium borohydride to the desired product. **Zr-1** was prepared following well-established solvothermal synthetic methods[12a,14] by the reaction of **L-1** with ZrCl$_4$ in dimethylformamide (DMF) in a closed vial at 120 °C using acetic acid as the reaction modulator. As will be discussed below, the incorporation of the pendant benzylamino groups of **L-1** within the structure of **Zr-1** ensures that the material's pores are lined with functional groups which possess both a π-electron-rich system and Brønsted basicity. To use this material as a fluorescent sensor for nitrophenols, we treated **Zr-1** with 4.0 M HCl for 8 h to protonate the material's secondary amino groups to ArRNH$_2$$^+$ Cl$^-$, to produce a cationic and π-electron rich framework with exchangeable Cl$^-$ anions (**pZr-1**) thus forming a favourable environment for hosting π-electron deficient and anionic nitroaromatic guests such as nitrophenol anions.

It has been observed by many researchers that ligands which are based on N-alkyl substituted 2-aminoterephthalic acid, often show various degrees of elimination of the alkyl substituent to form the parent ligand during MOF synthesis.[15] Therefore, in order to examine the stability of **L-1** once it is incorporated into the framework of **Zr-1**, we measured the ^{1}H-NMR spectra of digested MOF samples in D$_2$O/NaOD both before and after acid activation. As seen in Fig. S5 (ESI†), the spectrum of the digested as-synthesized MOF clearly shows the ^{1}H-NMR signals corresponding to **L-1** along with weak signals due to 2-aminoterephthalate (NH$_2$bdc^{2-}) indicating less than 10% elimination of the benzyl groups. However, ^{1}H-NMR spectra of digested samples of **pZr-1**, showed increased signals due to 2-aminoterephthalate. After conducting protonations of **Zr-1** with different HCl concentrations and reaction times, we found that the use of 4.0 M HCl for 8 h produces highly active **pZr-1** in terms of nitrophenol sensing, with ca. 30% benzyl group elimination (Fig. S7, ESI†). Thus, **pZr-1** henceforth refers to the activated material produced under these conditions. In accordance with the ^{1}H-NMR and thermogravimetric (see next section) analysis of **Zr-1** and **pZr-1**, the MOF formula is proposed to be {Zr$_6$O$_4$(OH)$_8$(H$_2$O)$_4$(**L-1**)$_{4-x}$(NH$_2$bdc)$_x$} (x = 0.4–1.2).

Scheme 1 Schematic representation of the synthesis of ligand **L-1** and MOF **Zr-1**.

12308 | J. Mater. Chem. C, 2022, **10**, 12307–12315
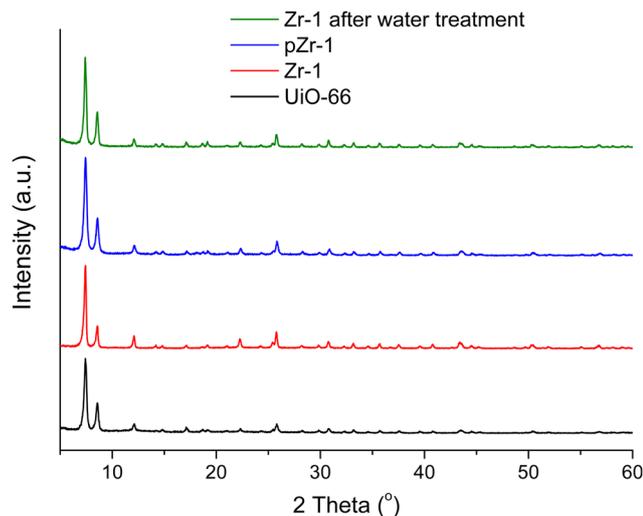
This journal is © The Royal Society of Chemistry 2022

Fig. 1 PXRD patterns of UiO-66 (black line), **Zr-1** (red line), **pZr-1** (blue line) and **Zr-1** after water treatment (green line).

Fig. 2 TGA curve for **Zr-1** after water treatment, under air.

Powder X-ray diffraction (PXRD) patterns of as synthesized **Zr-1**, **pZr-1** and the parent material UiO-66 can be seen in Fig. 1. All 2θ peaks of the diffraction pattern of **Zr-1** are consistent with UiO-66, which demonstrates that the two materials are structurally equivalent. However, as will be discussed below, the average connectivity of **Zr-1** is reduced to 8 compared to the 12-connectivity[12a] of UiO-66.

Chemical and thermal stability

Stability in water is a prerequisite for the potential application of a material in pollutant detection processes in aqueous environments. The stability of **Zr-1** towards H_2O was studied by treating the material with H_2O for 24 h at room temperature.

After treatment, the solid was isolated *via* centrifugation and dried at 50 °C for 24 h before PXRD analysis was performed. The PXRD pattern of **Zr-1** after water treatment is identical to the PXRD pattern of the as-synthesized material (Fig. 1). Evidently, the overall framework remains unaltered confirming that **Zr-1** displays high stability in aqueous environment.

The thermogravimetric analysis (TGA) curve for **Zr-1** after H_2O exchange is seen in Fig. 2. TGA analysis of the water treated sample under air reveals that **Zr-1** loses weight in two distinct steps: the first is completed at *ca.* 200 °C, and is attributed to the loss of lattice and coordinated water molecules, while the second, which is completed at *ca.* 550 °C, corresponds to complete ligand loss and formation of ZrO_2[12b,16] (see ESI† for details). It is interesting to mention that **Zr-1** exhibits a much lower weight loss due to the removal of water in comparison to what is observed for UiO-66-NH$_2$ (*ca.* 10% *vs.* 30%, Fig. S10, ESI†). This is attributed to the presence of benzyl side groups in **Zr-1**, which (i) decrease the free volume within the material's pores and (ii) render the material less hydrophilic. In contrast to **Zr-1**, HCl treated **pZr-1** shows a more extensive initial weight loss due to (i) an increased water content because of the partial elimination of benzyl side groups (*vide supra*) and (ii) the possible additional elimination of HCl (Fig. S10, ESI†).
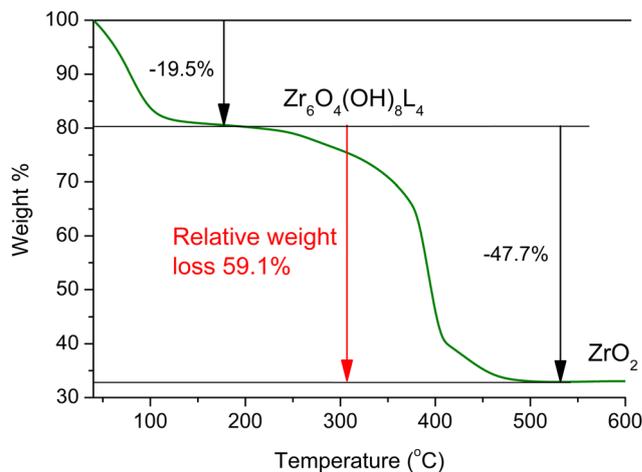
Assuming 10% cleavage of the benzyl side group (as estimated by ^{1}H-NMR analysis on digested **Zr-1**), we would expect a 12-connected material to have the formula $\{Zr_6O_4(OH)_8(H_2O)_4$-$(\textbf{L-1})_{5.4}(NH_2\text{-bdc})_{0.6}\}$, while an 8-connected material would have the formula $\{Zr_6O_4(OH)_8(H_2O)_4(\textbf{L-1})_{3.6}(NH_2\text{-bdc})_{0.4}\}$. Thus, the expected relative weight loss from 200 to 600 °C is expected to be 68.1% and 58.7% in the case of 12- and 8-connectivity, respectively. Based on the above, the experimentally determined 59.1% relative weight loss (Fig. 2) agrees with **Zr-1** having an average connectivity of 8. The missing linker defects of our material can be attributed to the steric hindrance induced by the bulky side group of ligand **L-1**. The lower connectivity of **Zr-1** possibly accounts for its lower decomposition temperature (~390 °C) compared to that observed for UiO-66 (>500 °C).[12a] The presence of missing-linker defects is a common feature of UiO-66(Zr)-type MOFs and defective materials reported in literature retain high crystallinity and thermal stability,[17] as is also observed in our work.

BET surface area and porosity

To evaluate the porosity and specific surface area, we performed N_2 adsorption–desorption measurements (77 K) on both **Zr-1** and **pZr-1** (Fig. 3). Both isotherms can be classified as Type I physisorption isotherms, typical of microporous materials.[18] The surface area was calculated by the Brunauer–Emmett–Teller (BET) model to 893 m^2 g^{-1} for **Zr-1** and 932 m^2 g^{-1} after activation with 4.0 M HCl (**pZr-1**). These values fall within the range of surface area values calculated for functionalized UiO-66-type materials prepared with solvothermal reactions.[19] The partial benzyl group cleavage that occurs during MOF activation possibly accounts for the slightly higher surface area determined for **pZr-1**. For comparison, we performed the same measurement on a sample of UiO-66-NH$_2$,[20] the 12-connected amino derivative of UiO-66, (Fig. S11, ESI†) and the BET surface area was determined to be 1274 m^2 g^{-1}, in good agreement with literature results[20b,21] The more open framework due to the 8-connectivity of **Zr-1** partially compensates for the presence of the bulky benzyl side

This journal is © The Royal Society of Chemistry 2022

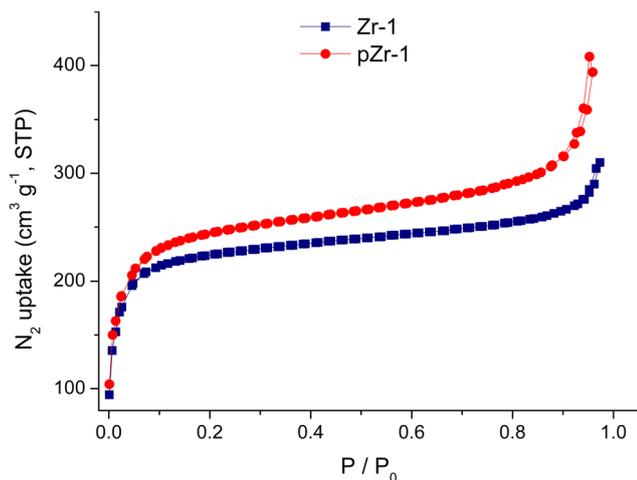*J. Mater. Chem. C*, 2022, **10**, 12307–12315 | **12309**

Fig. 3 Nitrogen sorption isotherms at 77 K of **Zr-1** and **pZr-1** after treatment with acetone and overnight evacuation (120 °C).
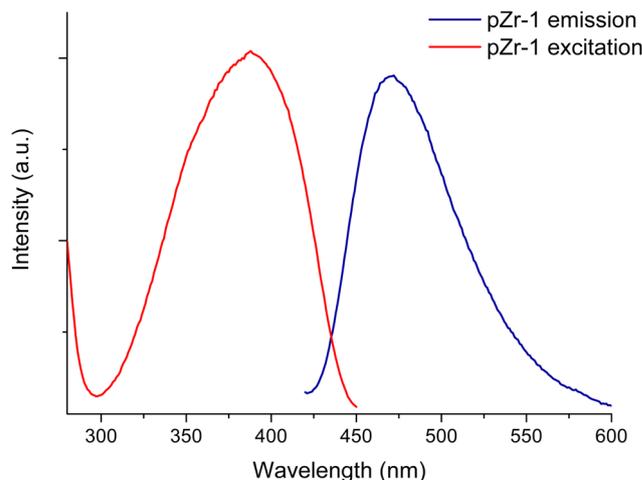

Fig. 4 Excitation and emission spectra (λ_{exc} = 400 nm) of **pZr-1** suspended in H_2O (0.1 mg mL^{-1}).

group thereby resulting in a BET surface area which is not dramatically lower than that of UiO-66-NH_2.

Photophysical properties

As described in the Experimental Part, **Zr-1** was treated with 4.0 M HCl prior to its use in sensing studies. Acid activation is an essential step to achieve detection of nitrophenols. The pK_a values for TNP and DNP are 0.3 and 4.0, respectively, indicating that the analyte molecules are found in their deprotonated form in the aqueous environment of the MOF suspension (pH = 4.5). Treatment with HCl ensures that the MOF's secondary amine units are protonated and introduces exchangeable Cl^- counter-ions. Combined, these features yield a favourable environment inside the MOF's pores so that the material can function as an ion exchange sensor for the anionic nitrophenols.

The activated material **pZr-1** readily forms a fine suspension in water and exhibits turquoise fluorescence upon selective ligand excitation at 400 nm. To examine the stability of the suspension we repeated multiple fluorescence measurements on a suspension of **pZr-1** in H_2O (0.1 mg mL^{-1}) in the span of 1.5 h and as can be seen in Fig. S12 (ESI†), the emission spectrum remains unaltered. Our group has previously reported the capability of a similar protonated Zr^{4+}-terephthalate MOF (**MOR-2**) to form fine and stable suspensions.[13]

The emission spectrum of **pZr-1** consists of a broad band with maximum at 470 nm (Fig. 4), similar to the emission spectrum of ligand **L-1** (Fig. S13, ESI†). The excitation spectrum of **pZr-1** (Fig. 4) consists of a broad band with a maximum at 370 nm that shows good agreement with the UV-vis absorption band of **L-1** (Fig. S13, ESI†) and with what is observed in UiO-66-NH_2(Zr/Hf)-type MOFs.[3b] The emission quantum yields of aqueous suspensions of **Zr-1** and **pZr-1** were found to be *ca.* 1.2% (Fig. S14 and S15, ESI†), double compared to that of a suspension of UiO-66-NH_2 (*ca.* 0.56%, Fig. S16, ESI†). The emission quantum yields of MOFs are much lower than those of the free ligands in methanol solution (Φ_{L-1} = 39%; Φ_{NH_2bdc} = 62%, Fig. S17 and S18, ESI†). This can be attributed to

self-quenching phenomena due to the relative proximity of the chromophores within the MOF matrix.[7a] The latter assumption is further supported by the much higher emission intensity displayed by the 8-connected **pZr-1** compared to the 12-connected UiO-66-NH_2, despite the free ligand NH_2bdc having a higher quantum yield than **L-1**. Despite its modest fluorescence quantum yield, **pZr-1** (aqueous suspension 0.1 mg mL^{-1}) displays a clear fluorescence signal which can be recorded easily and accurately. This phenomenon has also been observed in MOFs that emit in the near IR region and has been attributed to the large number of luminophores per unit volume enabling the material to emit a large number of photons thereby leading to a clear and strong emission signal which is suitable for sensing and imaging studies.[22]

It has been demonstrated, through electron paramagnetic resonance, time-resolved absorption spectroscopy and theoretical calculations, that the fluorescent excited state in Zr^{4+} MOFs with 2-aminoterephtahlate as bridging ligand predominantly involves shift of electron density from an orbital which is largely localized on the amino group to an unoccupied antibonding orbital of the aromatic ring without an appreciable contribution from a ligand-to-metal-charge-transfer (LMCT) component.[23] This type of intraligand charge transfer (ILCT) transitions show sensitivity to the local environment around the chromophore, such as the presence of hydrogen bond donors and/or electron accepting/donating moieties, and are thus well suited for optical sensing applications.[3b,9a,24]

Fluorescence titrations

Benefitting from the stability in water and its strong emission signal, we investigated the ability of **pZr-1** to sense trace amounts of nitrophenols in aqueous media. To evaluate the sensing ability of the material, we performed fluorescence titration experiments with gradual addition of aqueous solutions (5.0×10^{-5} M) of TNP and DNP to a suspension of **pZr-1** in H_2O (0.1 mg mL^{-1}) at pH 4.5. It should be noted that we applied Inner Filter Effect (IFE) correction to all our experimental data (see ESI† for details). As can be seen in Fig. 5, fluorescence

measurements clearly demonstrate that TNP and DNP have a strong quenching effect on the initial emission intensity of **pZr-1**, up to 92% and 86% at the end of the titration, respectively. For both titration experiments, the calibration curves show good linearity with respect to analyte concentration up to *ca.* 250 ppb. Through analysis of the linear fitting, we determined the Limits of Detection (LOD) and Quantification (LOQ) (see ESI† for details). LOD and LOQ values were calculated to be 0.011 and 0.037 μM (2.5 and 8.5 ppb) for TNP and 0.026 and 0.086 μM (4.8 and 16.0 ppb) for DNP detection, respectively. These values demonstrate that **pZr-1** exhibits effective sensing behaviour towards TNP and DNP in aqueous solutions.

The pores of **pZr-1** are lined with π-electron rich units which are potentially suitable for donor–acceptor association with the electron-deficient nitroaromatic compounds. Furthermore, we theorize that entry of analytes in the pores could be further assisted by H bonding interactions and electrostatic interactions between the positively charged protonated secondary amine units and the anionic nitroaromatic guests. An identical titration experiment with TNP carried out using **Zr-1**, the as synthesized material that is not fully protonated, produced non consistent results with higher LOD and LOQ values (0.030 μM and 0.139 μM, respectively). Additionally, the same experiment with a deprotonated MOF sample, treated with triethylamine/MeOH solution, resulted in much weaker fluorescence quenching. (Fig. S23, ESI†) These observations support our proposition that the MOF-analyte interaction has a strong electrostatic component.

To further examine the quenching efficiency, we analyzed the data with the Stern–Volmer equation, eqn (1)

$$(I_0/I) = 1 + K_{SV} \times [A] \qquad (1)$$

where I_0 and I are the integrated fluorescence intensities of **pZr-1** aqueous suspension before and after the addition of the analyte, respectively, K_{SV} is the quenching constant (M^{-1}) and $[A]$ is the molar concentration of the analyte.[25] The Stern–Volmer (SV) plots for both analytes (Fig. 5c) are nearly linear at low concentrations and show an upward curvature at higher concentrations. The non-linear nature of the Stern–Volmer plots is a characteristic feature observed when both static and dynamic quenching occurs for the same fluorophore. Therefore, it is reasonable we assume that quenching of **Zr-1** fluorescence is due to simultaneous presence of static and dynamic photoinduced electron transfer between **Zr-1** and the analytes. The static portion of the observed quenching can be attributed to stacking interactions between nitrophenols and the benzylamino groups inside the pores of **Zr-1**. Linear fitting of the SV plots at lower concentration range (0–2 μM) offer a quenching constant of 7.2×10^5 M^{-1} $(R^2 = 0.9995)$ for TNP and 2.9×10^5 M^{-1} $(R^2 = 0.9998)$ for DNP.

To further test our MOF's sensing performance, we performed detection experiments using a sample of acid activated UiO-66-NH$_2$, (Fig. S24 and S25, ESI†) and the results are shown in Table 1. Comparison of the fluorescence measurements for the two functionalized UiO-66-type MOFs demonstrates that **pZr-1** shows superior quenching response and sensitivity. The increased sensing ability of our MOF is the result of the strategical design that incorporates a π-electron-rich system
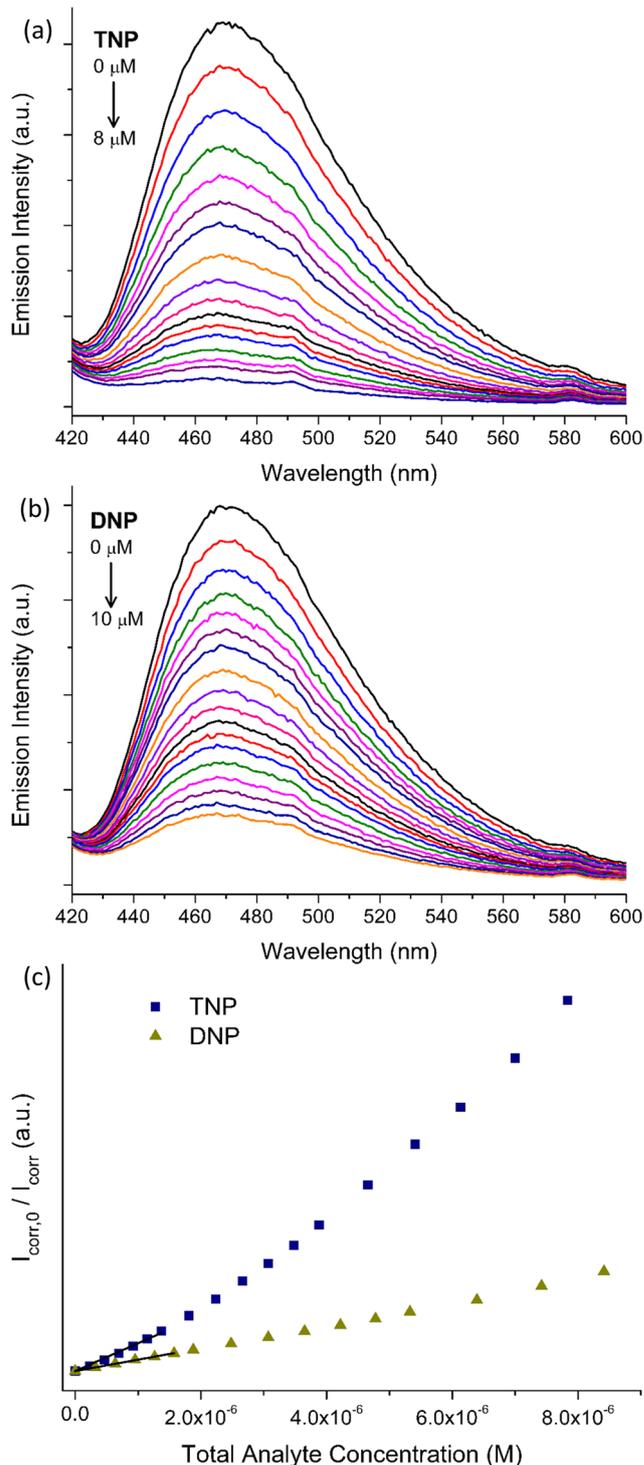

Fig. 5 Fluorescence titrations (λ_{exc} = 400 nm) of **pZr-1** suspended in H$_2$O (2 mL, 0.1 mg mL^{-1}) at pH 4.5 upon gradual addition of aqueous solution (5 × 10^{-5} M) of (a) TNP (b) DNP (c) Corresponding Stern–Volmer plots for both titrations, showing linearity at low analyte concentrations.

inside the MOF's pores, thus enhancing the interaction with electron deficient nitrophenolic analytes.

Detection of nitrophenols by luminescent MOF sensors has been reported in numerous studies over the last years.[10e] In

Table 1 LOD, LOQ and K_{SV} values calculated for fluorescence titrations (λ_{exc} = 380 nm) of acid activated UiO-66-NH$_2$ and **Zr-1** suspended in H$_2$O (0.1 mg mL^{-1}) at pH 4.5 upon gradual addition of aqueous solution of TNP and DNP. (IFE correction was applied to all experimental data)

	Analyte	LOD (μM)	LOQ (μM)	K_{SV} (M^{-1})	Maximum quenching %
UiO-66-NH$_2$	TNP	0.040	0.136	1.6×10^5	69
	DNP	0.042	0.140	1.7×10^5	64
pZr-1	TNP	0.011	0.037	7.2×10^5	92
	DNP	0.026	0.086	2.9×10^5	86

Table 2 we show LOD and LOQ values and K_{SV} values of some of the most efficient sensors reported. (A more extensive collection of representative recent examples can be found in Table S1, ESI†). Comparison of the data confirms that our material is among the best performing sensors and shows extremely high sensitivity. The LOD value for TNP (0.011 μM) is comparable with the lowest detection limit so far reported for TNP detection in H$_2$O, by Joarder *et al.* (12.9 nM).[27] The standout feature of **pZr-1** is that the material is hydrolytically stable and forms fine and stable suspension in water and, thus, can be used in analysis of aqueous samples. Furthermore, the λ_{exc} (400 nm) used in titration experiments lies in lower energy than the absorption maximum region of nitrophenols and the emission maximum of **pZr-1** does not overlap with the analytes' absorption bands, ensuring that the inner filter effect on the emission measurements is kept at a minimum.

Encouraged by these results we investigated the sensing selectivity of **pZr-1** towards DNP and TNP. We performed fluorescence measurements to examine the quenching efficiency towards several competing non-acidic compounds, including nitrobenzene (NB) 1,3-dinitrobenzene (1,3-DNB), 2-nitrotoluene (2-NT), 4-nitrotoluene (4-NT), 2,4-dinitrotoluene (DNT), 2,6-dinitrotoluene (2,6-DNT), 2-nitrophenol (2-NP), 3-nitrophenol (3-NP), 4-nitrophenol (4-NP), aniline (NA) and 3-nitroaniline (3-NA). The bar graphs in Fig. 6, illustrate the fluorescence response suspensions of activated **pZr-1** in H$_2$O (pH = 4.5) in the presence of competing compounds. These non-acidic compounds have a negligible quenching effect compared to the strong quenching observed upon subsequent addition of equal amounts of TNP or DNP (IFE correction was applied to all experimental data).

To further investigate our MOF's selectivity, we carried out fluorescence titration experiments with the above compounds (Fig. S26, ESI†). The S–V plots of these titrations are shown in Fig. 7 along with those for TNP and DNP. In addition to the expected low quenching effect, the competing compounds
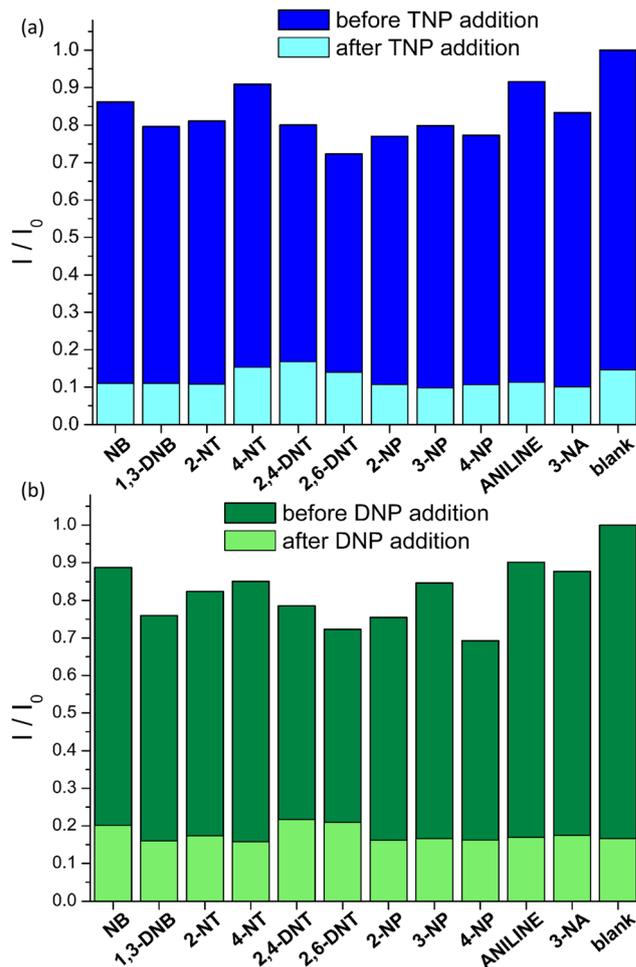

Fig. 6 Normalized fluorescence response I/I_0 (λ_{exc} = 400 nm) of **Zr-1** suspended in H$_2$O (2 mL, 0.1 mg mL^{-1}) at pH 4.5 in the presence of various analytes (12 μM) The dark bars represent the response in the presence of competing analytes and the light bars represent the response upon addition of (a) TNP (10 μM) and (b) DNP (12 μM). I_0 corresponds to emission intensity before the addition of analytes.

produce strictly linear S–V plots within the studied concentration range. This series of fluorescence measurements with a range of different analytes clearly demonstrates that **pZr-1** offers a remarkable combination of sensitivity and selectivity towards TNP and DNP. The lack of quenching response in the presence of mono-nitrophenols can be explained by considering that the pK_a values of these molecules are in the range 7.0–8.3, meaning that the hydroxylic groups are not deprotonated in the aqueous MOF suspension.

Table 2 Representative examples of some of the most efficient luminescent MOF sensors for TNP and DNP

Luminescent MOF	Analyte	Solvent	LOD (μM)	K_{SV} (M^{-1})	λ_{exc} (nm)	$\lambda_{em,max}$ (nm)	Ref.
[Zn$_2$(TCPE)(tta)$_2$]·2DMF·4H$_2$O·2Me$_2$NH$_2$$^+$	TNP	DMF	0.036	3.06×10^4	392	461	26
	DNP		0.029	3.75×10^4			
[Zn$_8$(ad)$_4$(BPDC)$_6$O·2Me$_2$NH$_2$]·G	TNP	H$_2$O	0.012	4.6×10^4	340	405	27
Zr$_6$O$_4$(OH)$_8$(H$_2$O)$_4$(TTNA)$_{8/3}$	TNP	H$_2$O	0.043	5.1×10^5	324	399	28
{Zr$_6$O$_4$(OH)$_8$(H$_2$O)$_4$(**L-1**)$_{4-x}$(NH$_2$bdc)$_x$}	TNP	H$_2$O	0.011	7.2×10^5	400	470	This work
	DNP	H$_2$O	0.026	2.9×10^5			

12312 | *J. Mater. Chem. C*, 2022, **10**, 12307–12315

This journal is © The Royal Society of Chemistry 2022

The treatment of **pZr-1** with saturated aqueous solutions of TNP and DNP (*ca.* 10^{-3} M) results in an instant color change from yellow to orange. After washing with MeOH to remove any loosely attached DNP or TNP, we digested the samples in 40% NaOD in D_2O, to perform ^{1}H-NMR analysis. The ^{1}H-NMR spectra confirmed the presence of the analytes within **Zr-1** (Fig. S28 and S30, ESI†) with peak area analysis showing guest-to-bridging ligand molar ratios of *ca.* 0.14 for TNP and *ca.* 0.22 for DNP. The higher molar ratio that we observed for the DNP guest could be attributed to a size effect. When we performed an analogous experiment in the concurrent presence of both analytes (*ca.* 10^{-3} M), subsequent ^{1}H-NMR analysis (Fig. S32, ESI†) showed that the material was loaded with equal amounts of TNP and DNP, thus reflecting their solution ratio. (The low solubility of DNP prevented us from performing further experiments at higher concentrations.)

Comparison of the PXRD pattens and IR spectra of **pZr-1** before and after being loaded with DNP and TNP confirm the material's structural stability upon its interaction with the analytes (Fig. S27, S29, S31 and S34, ESI†). It is worth noting that the IR spectrum of **pZr-1** shows the characteristic broad signal in the 3000–3800 cm^{-1} region due to absorbed water. In line with water molecules being displaced by the guest analyte, the water signal is greatly decreased in DNP-loaded **pZr-1** revealing the characteristic peak at 3382 cm^{-1} due to the NH stretch of the secondary amino groups (Fig. S33, ESI†).

To quantify the kinetic response of **pZr-1** towards TNP we performed a kinetic fluorescence scan (Fig. 8) where TNP was added to a suspension of **pZr-1**. The data could be satisfactorily fitted to two pseudo-first order processes[29] with time constants of 5.17(2) and 48.2(3) s, with the faster process having a far greater contribution (Fig. S36, ESI†). Thus, the material's fluorescence response to the presence of TNP is dominated by fast kinetics, as is desirable for an effective chemosensor.[30]
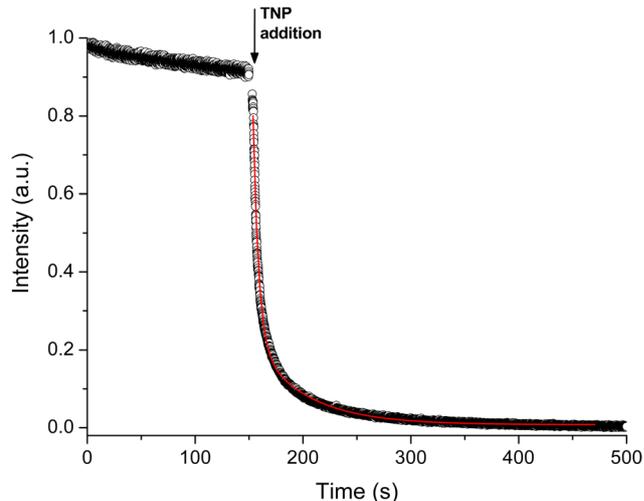

Fig. 8 Time-dependent fluorescence response (λ_{exc} = 400 nm, λ_{em} = 470 nm) of **pZr-1** suspended in H_2O (2 mL, 0.1 mg mL^{-1}) at pH 4.5 upon addition of 25 μL an aqueous solution of TNP (10^{-3} M). The concentration of TNP corresponds to that at the end of a typical titration experiment (8 μM). Black circles represent experimental data, the red curve represents the best fit based on a biexponential decay.

To evaluate the structural integrity and reusability of **Zr-1**, we examined the sensing ability of an activated MOF sample that was treated with TNP aqueous solution and re-activated. Fig. S34 (ESI†) displays the PXRD patterns of **pZr-1** after TNP sorption and reactivation confirming that the material retains good crystallinity apart from some minor. As shown in Fig. S35 (ESI†), fluorescence titration with gradual addition of TNP (5.0×10^{-5} M) on a suspension of the recycled sample in H_2O (2 mL, 0.1 mg mL^{-1}) resulted in quenching efficiency up to 89% with a quenching constant of 4.5×10^{-5} M^{-1}. Thus, we observe that after one cycle of analyte sorption and re-activation, the quenching constant value of **pZr-1** is slightly reduced, albeit the regenerated material still exhibits strong quenching in the presence of TNP.
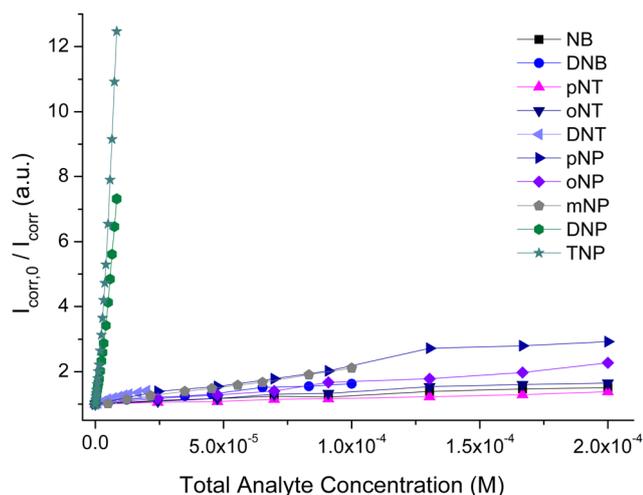
Conclusions

We have presented the synthesis and study of a porous Zr(IV) MOF (**Zr-1**) incorporating a bridging ligand (**L-1**) with a pendant benzylamino group, thereby creating a π-electron rich and basic environment within the material's pores, which is favourable for the hosting of acidic nitroaromatic guest species. Powder X-ray diffraction and thermogravimetric analysis showed that **Zr-1** possesses a UiO-66 type structure with a lower average connectivity of 8, compared to the 12-connectivity of UiO-66. This lower connectivity may be attributed to the bulky side groups on **L-1**, which prevent a closer approach between the bridging units. The N_2 adsorption isotherm of **Zr-1** corresponds to a BET surface area of 893 m^2 g^{-1}, indicating that the lower average connectivity combined with the partial cleavage (*ca.* 10%) of the benzyl side groups has a beneficial effect on the material's porosity. The material retains its structural integrity

Fig. 7 Comparison of Stern–Volmer plots of fluorescence titrations (λ_{exc} = 400 nm) of **pZr-1** suspended in H_2O (2 mL, 0.1 mg mL^{-1}) at pH 4.5 with different nitroaromatic analytes.

This journal is © The Royal Society of Chemistry 2022

J. Mater. Chem. C, 2022, **10**, 12307–12315 | **12313**

after protonation with 4.0 M HCl to yield **pZr-1**, which has a BET surface area of 932 $m^2 g^{-1}$, a small increase compared to as synthesized **Zr-1**, partly attributed to the increased cleavage of the benzyl side groups (reaching *ca.* 30% after protonation). When **pZr-1** is treated with aqueous solutions of TNP and DNP (10^{-3} M), we observe a darkening of the material's colour and the presence of analytes within the material is confirmed through ^{1}H-NMR analysis. Fluorescence titrations of aqueous suspensions of **pZr-1** with TNP and DNP lead to a strong quenching effect (92% and 86% by the end of the titration, respectively) with good signal linearity for analyte concentrations of up to *ca.* 250 ppb. We determined limits of detection and quantification of 0.011 and 0.037 μM for TNP, and 0.026 and 0.086 μM for DNP, respectively. Comparison with literature data places our material among the most efficient fluorescence sensors for the above analytes. It is important to emphasize that the excitation wavelength used in our studies (400 nm) is offset form the region of maximum absorption of DNP and TNP, thereby minimizing inner filter effects. We have confirmed this by observing insignificant alterations to the initial titration data after applying inner-filter corrections. Research on fluorescent metal–organic frameworks for the detection of nitroaromatic compounds is ongoing in our group.

Conflicts of interest

There are no conflicts to declare.

Acknowledgements

Notes and references

1 (*a*) V. Purohit and A. K. Basu, *Chem. Res. Toxicol.*, 2000, **13**, 673–692; (*b*) J. D. Rodgers and N. J. Bunce, *Water Res.*, 2001, **35**, 2101–2111; (*c*) P.-G. Rieger, H.-M. Meier, M. Gerle, U. Vogt, T. Groth and H.-J. Knackmuss, *J. Biotech.*, 2002, **94**, 101–123; (*d*) Z. C. Symons and N. C. Bruce, *Nat. Prod. Rep.*, 2006, **23**, 845–850; (*e*) K.-S. Ju and R. E. Parales, *Microbiol. Mol. Biol. Rev.*, 2010, **74**, 250–272; (*f*) P. Kovacic and R. Somanathan, *J. Appl. Toxicol.*, 2014, **34**, 810–824.

2 (*a*) D. S. Moore, *Rev. Sci. Instrum.*, 2004, **75**, 2499–2512; (*b*) S. Singh, *J. Hazard. Mater.*, 2007, **144**, 15–28; (*c*) M. E. Germain and M. J. Knapp, *Chem. Soc. Rev.*, 2009, **38**, 2543–2555.

3 (*a*) X. Sun, Y. Wang and Y. Lei, *Chem. Soc. Rev.*, 2015, **44**, 8019–8061; (*b*) W. P. Lustig, S. Mukherjee, N. D. Rudd, A. V. Desai, J. Li and S. K. Ghosh, *Chem. Soc. Rev.*, 2017, **46**, 3242–3285; (*c*) T. L. Mako, J. M. Racicot and M. Levine, *Chem. Rev.*, 2019, **119**, 322–477; (*d*) L. You, D. Zha and E. V. Anslyn, *Chem. Rev.*, 2015, **115**(15), 7840–7892; (*e*) M. D. Allendorf, R. Dong, X. Feng, S. Kaskel, D. Matoga and V. Stavila, *Chem. Rev.*, 2020, **120**(16), 8581–8640.

4 (*a*) J.-S. Yang and T. M. Swager, *J. Am. Chem. Soc.*, 1998, **120**, 5321–5322; (*b*) J.-S. Yang and T. M. Swager, *J. Am. Chem. Soc.*, 1998, **120**, 11864–11873.

5 (*a*) D. T. McQuade, A. E. Pullen and T. M. Swager, *Chem. Rev.*, 2000, **100**, 2537–2574; (*b*) S. W. Thomas, G. D. Joly and T. M. Swager, *Chem. Rev.*, 2007, **107**, 1339–1386; (*c*) O. P. Dimitriev, *Chem. Rev.*, 2022, **122**(9), 8487–8593.

6 S. Shanmugaraju and P. S. Mukherjee, *Chem. Commun.*, 2015, **51**, 16014–16032.

7 (*a*) M. Gutiérrez, R. Navarro, F. Sánchez and A. Douhal, *Phys. Chem. Chem. Phys.*, 2017, **19**, 16337–16347; (*b*) A. Sharma, D. Kim, J.-H. Park, S. Rakshit, J. Seong, G. H. Jeong, O.-H. Kwon and M. S. Lah, *Commun. Chem.*, 2019, **2**, 39; (*c*) G. Mercuri, G. Giambastiani and A. Rossin, *Inorganics*, 2019, **7**, 144; (*d*) D. J. Cerasale, D. C. Ward and T. L. Easun, *Nat. Rev. Chem.*, 2022, **6**, 9–30.

8 H. Furukawa, K. E. Cordova, M. O'Keeffe and O. M. Yaghi, *Science*, 2013, **341**, 1230444.

9 (*a*) S. A. Diamantis, A. Margariti, A. D. Pournara, G. S. Papaefstathiou, M. J. Manos and T. Lazarides, *Inorg. Chem. Front.*, 2018, **5**, 1493–1511; (*b*) C. R. Martin, P. Kittikhunnatham, G. A. Leith, A. A. Berseneva, K. C. Park, A. B. Greytak and N. B. Shustova, *Nano Res.*, 2021, **14**, 338–354; (*c*) C. R. Martin, K. C. Park, R. E. Corkill, P. Kittikhunnatham, G. A. Leith, A. Mathur, S. L. Abiodun, A. B. Greytak and N. B. Shustova, *Faraday Discuss.*, 2021, **231**, 266–280.

10 (*a*) X. Fang, B. Zong and S. Mao, *Nano-Micro Lett.*, 2018, **10**, 64; (*b*) L. Liu, X. Chen, J. Qiu and C. Hao, *Dalton Trans.*, 2015, **44**, 2897–2906; (*c*) Y. Zhang, S. Yuan, G. Day, X. Wang, X. Yang and H.-C. Zhou, *Coord. Chem. Rev.*, 2018, **354**, 28–45; (*d*) M.-L. Hu, S. A. A. Razavi, M. Piroozzadeh and A. Morsali, *Inorg. Chem. Front.*, 2020, **7**, 1598–1632; (*e*) T. Zhao, F. Zhang, J. Zhou and X. Zhao, *Comments Inorg. Chem.*, 2021, **41**, 100–132.

11 (*a*) T. K. Kim, J. H. Lee, D. Moon and H. R. Moon, *Inorg. Chem.*, 2013, **52**, 589–595; (*b*) D. Liu, K. Lu, C. Poon and W. Lin, *Inorg. Chem.*, 2014, **53**, 1916–1924; (*c*) A. Azhdari Tehrani, H. Ghasempour, A. Morsali, G. Makhloufi and C. Janiak, *Cryst. Growth Des.*, 2015, **15**, 5543–5547; (*d*) M. Bagheri, M. Y. Masoomi, A. Morsali and A. Schoedel, *ACS Appl. Mater. Interfaces*, 2016, **8**, 21472–21479; (*e*) Q.-Y. Li, Z. Ma, W.-Q. Zhang, J.-L. Xu, W. Wei, H. Lu, X. Zhao and X.-J. Wang, *Chem. Commun.*, 2016, **52**, 11284–11287; (*f*) B. Wang, X.-L. Lv, D. Feng, L.-H. Xie, J. Zhang, M. Li, Y. Xie, J.-R. Li and H.-C. Zhou, *J. Am. Chem. Soc.*, 2016, **138**, 6204–6216; (*g*) A. Azhdari Tehrani, L. Esrafili, S. Abedi, A. Morsali, L. Carlucci, D. M. Proserpio, J. Wang, P. C. Junk and T. Liu, *Inorg. Chem.*, 2017, **56**, 1446–1454; (*h*) L. Luconi, G. Mercuri, T. Islamoglu, A. Fermi, G. Bergamini, G. Giambastiani and A. Rossin, *J. Mater. Chem. C*, 2020, **8**, 7492–7500; (*i*) G. Mercuri, M. Moroni, S. Galli, C. Piccirillo, A.-L. Capodilupo, G. Tuci,

12314 | *J. Mater. Chem. C*, 2022, **10**, 12307–12315

This journal is © The Royal Society of Chemistry 2022

    G. Giambastiani and A. Rossin, *Inorg. Chem. Front.*, 2022, **9**, 90–102.

12 (*a*) J. H. Cavka, S. Jakobsen, U. Olsbye, N. Guillou, C. Lamberti, S. Bordiga and K. P. Lillerud, *J. Am. Chem. Soc.*, 2008, **130**, 13850–13851; (*b*) L. Valenzano, B. Civalleri, S. Chavan, S. Bordiga, M. H. Nilsen, S. Jakobsen, K. P. Lillerud and C. Lamberti, *Chem. Mater.*, 2011, **23**, 1700–1718.

13 S. Rapti, D. Sarma, S. A. Diamantis, E. Skliri, G. S. Armatas, A. C. Tsipis, Y. S. Hassan, M. Alkordi, C. D. Malliakas, M. G. Kanatzidis, T. Lazarides, J. C. Plakatouras and M. J. Manos, *J. Mater. Chem. A*, 2017, **5**, 14707–14719.

14 A. Schaate, P. Roy, A. Godt, J. Lippke, F. Waltz, M. Wiebcke and P. Behrens, *Chem. – Eur. J.*, 2011, **17**, 6643–6651.

15 (*a*) L. L. Keenan, H. A. Hamzah, M. F. Mahon, M. R. Warren and A. D. Burrows, *CrystEngComm*, 2016, **18**, 5710–5717; (*b*) A. Helal, M. Nasiruzzaman Shaikh and M. Abdul Aziz, *J. Photochem. Photobiol. A*, 2020, **389**, 112238.

16 A. D. Pournara, S. Rapti, A. Valmas, I. Margiolaki, E. Andreou, G. S. Armatas, A. C. Tsipis, J. C. Plakatouras, D. L. Giokas and M. J. Manos, *J. Mater. Chem. A*, 2021, **9**, 3379–3387.

17 Y. Feng, Q. Chen, M. Jiang and J. Yao, *Ind. Eng. Chem. Res.*, 2019, **58**, 17646–17659.

18 M. Thommes, K. Kaneko, A. V. Neimark, J. P. Olivier, F. Rodriguez–Reinoso, J. Rouquerol and K. S. W. Sing, *Pure Appl. Chem.*, 2015, **87**, 1051–1069.

19 G. E. Cmarik, M. Kim, S. M. Cohen and K. S. Walton, *Langmuir*, 2012, **28**, 15606–15613.

20 (*a*) M. Kandiah, M. H. Nilsen, S. Usseglio, S. Jakobsen, U. Olsbye, M. Tilset, C. Larabi, E. A. Quadrelli, F. Bonino and K. P. Lillerud, *Chem. Mater.*, 2010, **22**, 6632–6640; (*b*) S. Rapti, A. Pournara, D. Sarma, I. T. Papadas, G. S. Armatas, Y. S. Hassan, M. H. Alkordi, M. G. Kanatzidis and M. J. Manos, *Inorg. Chem. Front.*, 2016, **3**, 635–644.

21 (*a*) K. Užarević, T. C. Wang, S.-Y. Moon, A. M. Fidelli, J. T. Hupp, O. K. Farha and T. Friščić, *Chem. Commun.*, 2016, **52**, 2133–2136; (*b*) S. Subudhi, G. Swain, S. P. Tripathy and K. Parida, *Inorg. Chem.*, 2020, **59**, 9824–9837.

22 (*a*) K. White, D. Chengelis, K. Gogick, J. Stehman, N. Rosi and S. Petoud, *J. Am. Chem. Soc.*, 2009, **131**(50), 18069–18071; (*b*) A. Foucault-Collet, K. A. Gogick, K. A. White, S. Villette, A. Pallier, G. Collet, C. Kieda, T. Li, S. J. Geib, N. L. Rosi and S. Petoud, *Proc. Natl. Acad. Sci. U. S. A.*, 2013, **110**, 17199–17204; (*c*) Y. Cui, J. Zhang, H. He and G. Qian, *Chem. Soc. Rev.*, 2018, **47**, 5740–5785; (*d*) G. Collet, A. Hrvat, S. V. Eliseeva, C. Besnard, A. Kovalenko and S. Petoud, *Chem. Commun.*, 2021, **57**, 3351–3354.

23 (*a*) M. A. Nasalevich, C. H. Hendon, J. G. Santaclara, K. Svane, B. van der Linden, S. L. Veber, M. V. Fedin, A. J. Houtepen, M. A. van der Veen, F. Kapteijn, A. Walsh and J. Gascon, *Sci. Rep.*, 2016, **6**, 23676; (*b*) J. G. Santaclara, F. Kapteijn, J. Gascon and M. A. van der Veen, *CrystEngComm*, 2017, **19**, 4118–4125.

24 V. Balzani, P. Ceroni and A. Juris, *Photochemistry and Photophysics: Concepts, Research, Applications*, Wiley-VCH, Weinheim, Germany, 2014.

25 J. Keizer, *J. Am. Chem. Soc.*, 1983, **105**, 1494–1498.

26 X. Zhang, G. Ren, M. Li, W. Yang and Q. Pan, *Cryst. Growth Des.*, 2019, **19**, 6308–6314.

27 B. Joarder, A. V. Desai, P. Samanta, S. Mukherjee and S. K. Ghosh, *Chem. – Eur. J.*, 2015, **21**, 965–969.

28 B. Wang, X.-L. Lv, D. Feng, L.-H. Xie, J. Zhang, M. Li, Y. Xie, J.-R. Li and H.-C. Zhou, *J. Am. Chem. Soc.*, 2016, **138**, 62046216.

29 (*a*) S. Azizian, *J. Colloid Interface Sci.*, 2004, **276**, 47–52; (*b*) S. Douven, C. A. Paez and C. J. Gommes, *J. Colloid Interface Sci.*, 2015, **448**, 437–450.

30 L. Shi, N. Li, D. Wang, M. Fan, S. Zhang and Z. Gong, *Trends Anal. Chem.*, 2021, **134**, 116131.

This journal is © The Royal Society of Chemistry 2022

J. Mater. Chem. C, 2022, **10**, 12307–12315 | **12315**